THE JOURNAL OF PHYSICAL CHEMISTRY C

Article

pubs.acs.org/JPCC

# Colloidal Nanoplatelet/Conducting Polymer Hybrids: Excitonic and Material Properties

Burak Guzelturk,[†] Florian Menk,[‡] Kai Philipps,[‡] Yusuf Kelestemur,[†] Murat Olutas,[†,§] Rudolf Zentel,[‡] and Hilmi Volkan Demir*[,†,∥]

[†]Department of Electrical and Electronics Engineering, Department of Physics and UNAM−National, Nanotechnology Research Center, Institute of Materials Science and Nanotechnology, Bilkent University, TR-06800 Bilkent, Ankara, Turkey

[‡]Institute for Organic Chemistry, Johannes Gutenberg University, Duesbergweg 10-14, 55128 Mainz, Germany

[§]Department of Physics, Abant Izzet Baysal University, Bolu 14280, Turkey

[∥]Luminous! Center of Excellence for Semiconductor Lighting and Displays, School of Electrical and Electronic Engineering, School of Physical and Mathematical Sciences, School of Materials Science and Nanotechnology, Nanyang Technological University, Nanyang Avenue, Singapore 639798, Singapore

Supporting Information

**ABSTRACT:** Here we present the first account of conductive polymer/colloidal nanoplatelet hybrids. For this, we developed DEH-PPV-based polymers with two different anchor groups (sulfide and amine) acting as surfactants for CdSe nanoplatelets, which are atomically flat semiconductor nanocrystals. Hybridization of the polymers with the nanoplatelets in the solution phase was observed to cause strong photoluminescence quenching in both materials. Through steady-state photoluminescence and excitation spectrum measurements, photoluminescence quenching was shown to result from dominant exciton dissociation through charge transfer at the polymer/nanoplatelet interfaces that possess a staggered (i.e., type II) band alignment. Importantly, we found out that sulfide-based anchors enable a stronger emission quenching than amine-based ones, suggesting that the sulfide anchors exhibit more efficient binding to the nanoplatelet surfaces. Also, shorter surfactants were found to be more effective for exciton dissociation as compared to the longer ones. In addition, we show that nanoplatelets are homogeneously distributed in the hybrid films owing to the functional polymers. These nanocomposites can be used as building blocks for hybrid optoelectronic devices, such as solar cells.

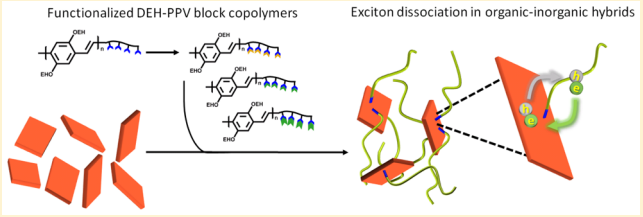


## 1. INTRODUCTION

Organic−inorganic hybrids comprising organic semiconductors and colloidal nanocrystals make an attractive combination of soft material systems for optoelectronic devices including solar cells[1−5] and light-emitting diodes.[5−11] Strong interest in hybrid materials stems, in particular, from their solution processability, which allows for fabrication of possibly large-area devices via low-cost printing and patterning techniques essentially on arbitrary substrates at large scale. There has been an ever-growing interest for this type of hybrid systems since the breakthrough achievement of Alivisatos' group reporting a hybrid solar cell composed of CdSe nanorods and poly(3-hexylthiophene) (P3HT) conjugated polymers.[1] Recent reports show that the power conversion efficiencies in the hybrid solar cells can attain over 5%.[12,13] Also, based on theoretical calculations, hybrid solar cells are predicted to achieve efficiencies that could possibly exceed 10% by employing optimized hybrid structures offering enhanced free carrier generation and charge transport.[14,15]

In a hybrid solar cell, exciton dissociation, charge transport, and charge extraction are the essential processes. Efficient free carrier generation via exciton dissociation requires assistance of exciton diffusion since excitons should reach the exciton dissociating interfaces before they would recombine.[16] Unfortunately, exciton diffusion in the colloidal nanocrystals and organic semiconductors is generally limited to short distances (<20 nm).[5] As a result of this limitation, it is commonly desired to realize nanoscale morphologies having very small domains on the order of exciton diffusion length so that free carrier generation could be maximized. In addition to nanoscale morphology, extrinsic and intrinsic properties of the inorganic nanocrystals, including their ligands, size, and geometry, also play a significant role in the free carrier generation efficiency and, thus, the overall solar cell efficiency in hybrid systems.[5,17]

Long alkyl chain-based insulating ligands of the nanocrystals restrict charge separation and transport in their solid films. In an early report, Geenham et al. described ligand modification of

**Received:** December 28, 2015
**Revised:** January 27, 2016
**Published:** January 27, 2016





DOI: 10.1021/acs.jpcc.5b12661
J. Phys. Chem. C 2016, 120, 3573−3582

CdSe quantum dots (QDs) that were primarily coated with insulating tri-*n*-octylphosphine oxide (TOPO) ligands by the treatment with an excess of pyridine.[16] Since then, various ligand modification procedures have been developed either using short organic or inorganic ligands.[10,15,18,19] However, ligand exchange does not simply change the QD/QD and QD/polymer distances; it also affects the conductivity, energy levels, stability, and the morphology of casted films.[20−22] Furthermore, some functional groups such as thiols are known to create charge traps in the nanocrystals and quench their photoluminescence.[23,24] Therefore, predicting the influence of a specific ligand on the optical properties of the hybrids is difficult and complex. Consequently, studies that separately investigate the influence on the individual aspects depending on both the size and the functional group of the ligands are required.

Morphology of the nanocrystals (i.e., size, shape, and dimensionality) is another important feature determining the performance of the organic−inorganic hybrids. To date, CdSe and CdS nanorods have shown favorable performance as compared to that of the colloidal QDs thanks to their large surface area and high aspect ratio, which considerably increases the overall free carrier generation efficiency at the organic−inorganic interfaces.[4,17,25] High-aspect-ratio organic materials such as conjugated polymer nanowires have been also previously shown to enhance the power conversion efficiencies through creating a nanoscale morphology favorable for charge separation and transport.[26]

Recently, a new type of colloidal semiconductor commonly known as colloidal nanoplatelets (NPLs), or alternatively colloidal quantum wells, has been introduced.[27] These NPLs are atomically flat nanocrystals that exhibit unique optical and material properties, including extremely large linear and nonlinear absorption cross sections, large oscillator strength, and narrow emission line width.[28,29] Thanks to these favorable properties, recent reports have shown that the NPLs are highly promising for the applications of light-emitting diodes,[30] lasers,[31,32] photodetectors,[33,34] and photocatalysis.[35] Moreover, ultraefficient exciton transfer has been shown to prevail in the close-packed solid films of the NPLs,[36,37] which is expected to facilitate long exciton diffusion lengths (>100 nm) in their solid films.[38] These long exciton diffusion lengths would clearly manifest the high potential of NPLs in light-harvesting applications. In addition, their high aspect ratio, large surface area, and anisotropic shape also make the NPLs interesting candidates for organic−inorganic hybrid systems. However, to date, there has been no demonstration or of any systematic study of organic−inorganic nanocomposites containing the NPLs and the conjugated polymers.

In this work, we proposed and demonstrated hybrid composites combining for the first time colloidal nanoplatelets and conjugated polymers. In this hybrid system, we studied different anchor groups of the conductive polymer to hybridize with CdSe NPLs. To this end, we developed DEH-PPV-based block copolymers having two ligands of varying size and anchor groups. Through investigation of steady-state optical properties of the hybrids in the solution phase, we revealed strong photoluminescence quenching in both the co-integrated polymers and the nanoplatelets. The emission quenching is well explained with exciton dissociation at the polymer/nanoplatelet interfaces having a staggered band alignment. Among different anchors, sulfides lead to the strongest quenching as attributed to their higher tendency to attach to the NPL surfaces. Also, a shorter ligand size of the same anchor group is shown to yield a larger photoluminescence quenching as compared to the ligands with a larger size. Furthermore, we observed that the hybridization helps to form well-dispersed NPL films as revealed by transmission electron microscopy, whereas the NPLs alone tend to form aggregated assemblies in the absence of functional polymers. The proposed hybrid composites with exciton dissociating interfaces and homogeneous NPL distribution are highly promising for making hybrid solar cells.

## 2. EXPERIMENTAL SECTION

**Materials and Characterization.** All commercially available chemicals were purchased from Alfa Aesar, Acros Organics, Fluka, Sigma-Aldrich, or Tokyo Chemical Industry and used without further purification unless otherwise noted. Anhydrous THF was freshly distilled from sodium at dry argon atmosphere. All reactions were carried out under dry argon using standard Schlenk line techniques unless otherwise noted. 2′,5′-Di(2″-ethylhexyloxy)-4′-methyl-*N*-benzylideneaniline (**1**) and the reactive ester block copolymer **P1** were synthesized according to a modified literature procedure.[1] $^1$H NMR and $^{19}$F NMR spectra were acquired on a Bruker ARX 400 at a Lamor frequency of 400 MHz. FTIR spectra were performed on a Vector 22 ATR-FTIR spectrometer made by Bruker. Molecular weights of all synthesized polymers were determined by gel permeation chromatography (GPC) with a concentration of 1.2 mg mL$^{-1}$ in THF with polystyrene as the external standard and toluene as the internal standard.

Cyclic voltammetry measurements were carried out on a drop-cast film at room temperature in a nitrogen glovebox. Platinum electrodes were used as working and counter electrodes. The reference electrode was an Ag/Ag$^+$ electrode, and the measurements were conducted in a 0.1 M solution of tetrabutylammonium hexafluorophosphate ($TBAPF_6$) as the supporting electrolyte in anhydrous acetonitrile. Ferrocene was used as an internal standard, and the energy levels were calculated from the onsets of the oxidation and reduction potential, respectively, with an assumed level of the Fc/Fc$^+$ redox couple of −5.1 eV versus the vacuum.

**General Procedure for Postpolymerization Modifications.** The precursor polymer **P1** (0.032 mmol, 1 equiv) was dissolved in 2.5 mL of dry THF under an argon atmosphere. The respective primary amine (0.476 mmol, 15 equiv) and triethylamine (0.476 mmol, 15 equiv) were added, and the reaction mixture was stirred at 30 °C for 48 h. Purification was achieved by precipitation in methanol and redissolving in DCM for three times.

**P2a**: $^1$H NMR (400 MHz, $CDCl_3$, $\delta$): 7.38−7.60 (m, 36H, Ar), 7.02−7.26 (m, 36H, CH═CH), 3.68−4.06 (m, 80H, O−$CH_2$), 2.60 (br, 8H, S−$CH_2$), 2.13 (br, 12H, S−$CH_3$), 1.17−1.86 (m, 336H, CH + $CH_2$), 0.82−1.05 (m, 222H, $CH_3$). $^{19}$F NMR (400 MHz, $CDCl_3$, $\delta$): no signals. FTIR: $\nu$ = 1676 cm$^{-1}$.

**P2b**: $^1$H NMR (400 MHz, $CDCl_3$, $\delta$): 7.38−7.56 (m, 36H, Ar), 7.02−7.24 (m, 36H, CH═CH), 3.65−4.02 (m, 80H, O−$CH_2$), 2.87 (br, 8H, N−$CH_2$), 2.23 (br, 24H, N−$CH_3$), 1.17−1.86 (m, 336H, CH + $CH_2$), 0.83−1.04 (m, 222H, $CH_3$). $^{19}$F NMR (400 MHz, $CDCl_3$, $\delta$): no signals. FTIR: $\nu$ = 1672 cm$^{-1}$.

**P2c**: $^1$H NMR (400 MHz, $CDCl_3$, $\delta$): 7.38−7.56 (m, 36H, Ar), 7.02−7.24 (m, 36H, CH═CH), 3.65−4.01 (m, 80H, O−$CH_2$), 2.84 (br, 8H, N−$CH_2$), 2.25 (br, 24H, N−$CH_3$), 1.17−1.86 (m, 352H, CH + $CH_2$), 0.83−1.03 (m, 222H, $CH_3$). $^{19}$F NMR (400 MHz, $CDCl_3$, $\delta$): no signals. FTIR: $\nu$ = 1668 cm$^{-1}$.


DOI: 10.1021/acs.jpcc.5b12661
J. Phys. Chem. C 2016, 120, 3573−3582

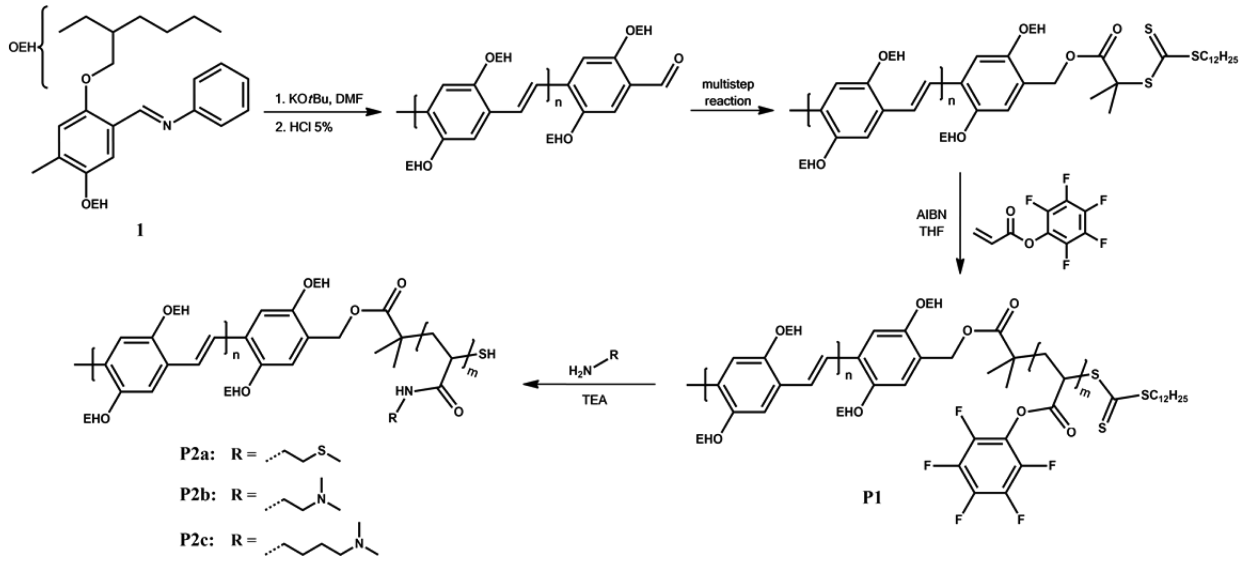


**Figure 1.** General reaction scheme for the incorporation of anchor groups into the block copolymer containing a conjugated DEH-PPV block and assignment of the polymers **P1** and **P2a−c**.

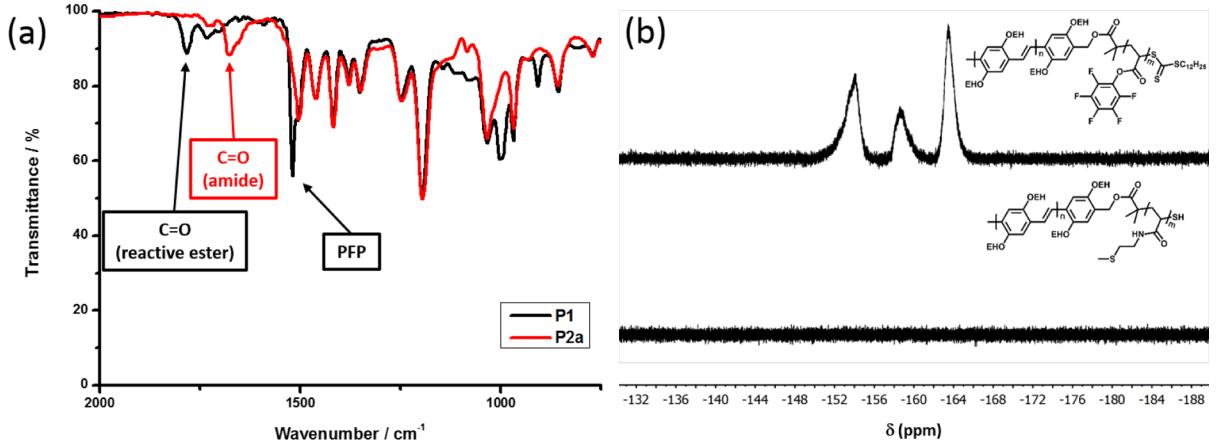


**Figure 2.** (a) FTIR spectra verifying the success of the postpolymerization modification and (b) $^{19}$F NMR spectra of polymers **P1** and **P2a**. While the signals of the reactive ester occur in the $^{19}$F NMR spectrum of precursor polymer **P1**, full conversion of the postpolymerization modification is evidenced by the absence of any signals in the spectrum of polymer **P2a**. (Spectra verifying the successful synthesis of polymers **P2b** and **P2c** can be obtained from Figures S4 and S6.)

**Synthesis of Four-Monolayer-Thick CdSe NPLs.** We used a synthesis recipe for the four-monolayer CdSe nanoplatelets based on our previous report.[38] Consequently, CdSe NPLs having a vertical thickness of four monolayers (1.2 nm) were synthesized together with other quantum dot populations as side products. To purify the NPLs and separate them from the quantum dots, we cleaned them via ultracentrifugation with the addition of acetone/ethanol mixture. The cleaning step was repeated few times, and the precipitate (i.e., purified NPLs) was then dissolved in toluene. The purity of the nanoplatelets was evidenced by the pure absorbance and photoluminescence spectra.

## 3. RESULTS AND DISCUSSION

Surfactants have a strong influence on the properties of organic−inorganic nanocomposites with regard to their optoelectronic performance and applications. As both the size and the functional group of a surfactant affect the properties, here we studied the influence of the two aspects separately. The required interaction of the inorganic nanocrystals and the conjugated polymer was accomplished by the incorporation of anchor groups into the polymer. These anchor groups were composed of a functional group targeted to enable an effective binding to the inorganic nanocrystals and a spacer that determined the distance between polymers and nanocrystals. Because of its favorable optoelectronic properties, the poly(*p*-phenylenevinylene) derivative DEH-PPV was selected as the conjugated block. DEH-PPV can be synthesized via Siegrist polycondensation, which offers a defined functional end group. This end group was further exploited for the incorporation of a second block, which is nonconjugated, composed of a reactive ester repeating unit via RAFT polymerization,[39] allowing for the incorporation of different anchor groups (see Figure 1). To guarantee that the observed differences in the properties originate from the varying anchor groups, all polymers employed in the study were synthesized from a single precursor polymer as illustrated in Figure 1. By exploiting only the same block copolymer architecture, influence of the anchor groups on the torsion and, thereby, photophysical properties of the conjugated backbone was also avoided. The precursor polymer


DOI: 10.1021/acs.jpcc.5b12661
*J. Phys. Chem. C* 2016, 120, 3573−3582

that does not have any anchor group is hereafter named as the reference polymer **P1**. The functional polymers with anchors based on sulfide is called **P2a**, and the ones based on amino are called **P2b** and **P2c**. The ligand size is the same in **P2a** and **P2b** polymers, while the spacer is longer in **P2c** (see Figure 1).

When incorporating anchor groups into a conjugated polymer, several aspects have to be taken into account. The incorporation of anchor groups as the side chains into the conjugated polymer backbone or as the end groups is usually relatively simple. Unfortunately, both approaches come along with disadvantages. The incorporation of anchor groups as the side chains disturbs the polymer's regioregularity, causes torsion in the backbone, and decreases the planarity of the conjugated backbone.[3,40] Also, with an increasing chain length of the polymer the possibility of a single functional end group to be in a suitable position for interacting with the nanocrystal surface is significantly decreased. In this latter case, only very strong anchor groups such as enediols in the case of $TiO_2$ nanoparticles could form stable coatings.[41,42] Therefore, the use of block copolymers, which we employ here, is highly desired since they both allow for multiple anchor groups and, thereby, enable the formation of a stable coating without sacrificing the original optoelectronic properties of the conjugated polymer owing to the separation of the conjugated block from the anchor groups. Therefore, torsion of the conjugated backbone does not occur. Since the combination of a conjugated PPV block and a nonconjugated block via one-pot block copolymerization can be solely achieved by applying ring-opening metathesis polymerization (ROMP), which involves complicated monomer synthesis, a synthetic route exploiting the defined end group installed via Siegrist polycondensation was applied in the study at hand.[39,43]

Successful incorporation of the anchor groups via post-polymerization modification is evidenced via FTIR spectroscopy. Upon incorporation of the anchor groups, the band originating from the pentafluorophenyl ring at 1519 $cm^{-1}$ disappears. Moreover, the C═O band shifts from 1783 $cm^{-1}$ in the reactive ester to approximately 1670 $cm^{-1}$ in the amides (see Figure 2a and Figures S2, S4, and S6). Full conversion of the postpolymerization modification is confirmed by the absence of any signals in the $^{19}F$ NMR spectra of the amides. In addition, the successful incorporation of the anchor groups is verified via $^{1}H$ NMR spectroscopy. After postpolymerization modification, the spectra of the polymers exhibit signals that can be assigned to the respective anchor group (see Figures S3, S5, and S7).

As the inorganic nanocrystals, we employ atomically flat CdSe NPLs having four monolayer (ML) vertical thickness (~1.2 nm). We chose 4 ML CdSe NPLs because of their well-established synthesis and increased stability. In Figure 3a, absorbance and photoluminescence (PL) spectra of the NPLs are shown (in solution phase). The absorbance of the NPLs exhibit two peaks that are at 480 and 512 nm arising from electron/light-hole and electron/heavy-hole transitions, respectively. The PL peak arises from the recombination of the excitons at the electron/heavy-hole transition (~513 nm). The emission line width in the NPLs is as narrow as ~8 nm due to absence of inhomogeneous broadening.[44] The inset in Figure 3a shows a high-angle annular dark-field scanning transmission electron microscopy (HAADF-STEM) image of the NPLs. In the STEM image, most of the NPLs can be seen lying flat on the TEM grid, while some of them can be observed to form stack-like assemblies, which lie perpendicular to the TEM grid.

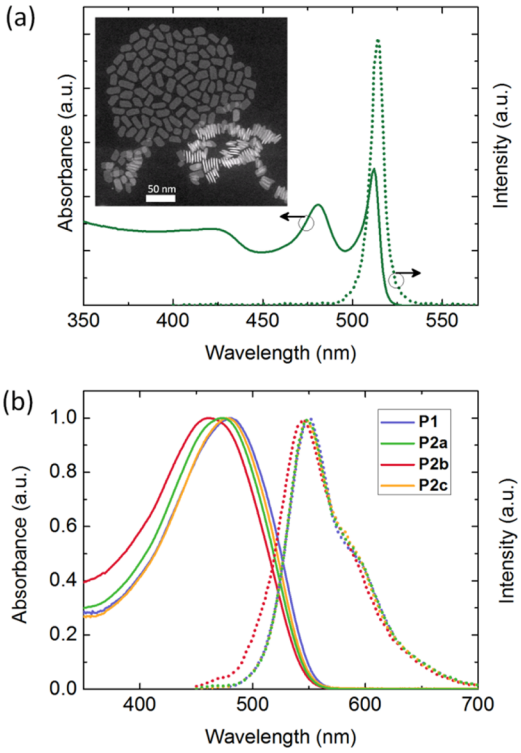


**Figure 3.** Absorbance (solid) and photoluminescence (dotted) of (a) 4 monolayer thick CdSe nanoplatelets and (b) conjugated polymers **P1** and **P2a−c**. Inset in (a) shows the HAADF-STEM image of the CdSe nanoplatelets; the scale bar is 50 nm.

The stacking of the NPLs is commonly observed in their solid films since the NPLs tend to assemble together in long chains due to strong van der Waals forces between their large and flat surfaces.[45] The absorbance and PL spectra of the conjugated polymers are also presented in Figure 3b. The PL peaks of the polymers are at ~550 nm, and their absorption peaks are at approximately at 460 nm. We observe very slight shifts between the absorbance and emission spectra of different polymers used here, which may arise from the use of different ligands.

We investigate the steady-state PL of the NPLs and the polymers when they are mixed together in the solution phase. For this, first, we prepared a dilute nanoplatelet solution in toluene. The absorbance of the initial NPL solution is very low (~0.1 at the first exciton peak 512 nm) to prevent reabsorption and concentration based energy transfer effects. The concentration of the NPLs is calculated to be 12.3 nM (in 3 mL of toluene) by using their reported absorption cross section.[44] Polymer solutions were prepared separately using toluene as the solvent with a concentration of 2 mg/mL. Then, step by step we added small amounts of a polymer into the NPL solution. Each step adds 5 $\mu$L of polymer solution into the NPL solution, which corresponds to addition of ~1.4 nmol for **P2a** and **P2b** polymers and ~1.3 nmol for **P1** in each step as calculated by their molecular weight (see Supporting Information).

As the polymer **P2a** (polymer with sulfide anchor) was added to the NPL solution, we observed that the NPL emission started to immediately decrease (see Figure 4a) when excited at 375 nm. In the case of polymer **P2b**, which carries an amine anchor with the same ligand size as in **P2a**, the decrease in the NPL emission was also evident (see Figure 4b). As more polymer was added step by step, the NPL emission was


DOI: 10.1021/acs.jpcc.5b12661
J. Phys. Chem. C 2016, 120, 3573−3582

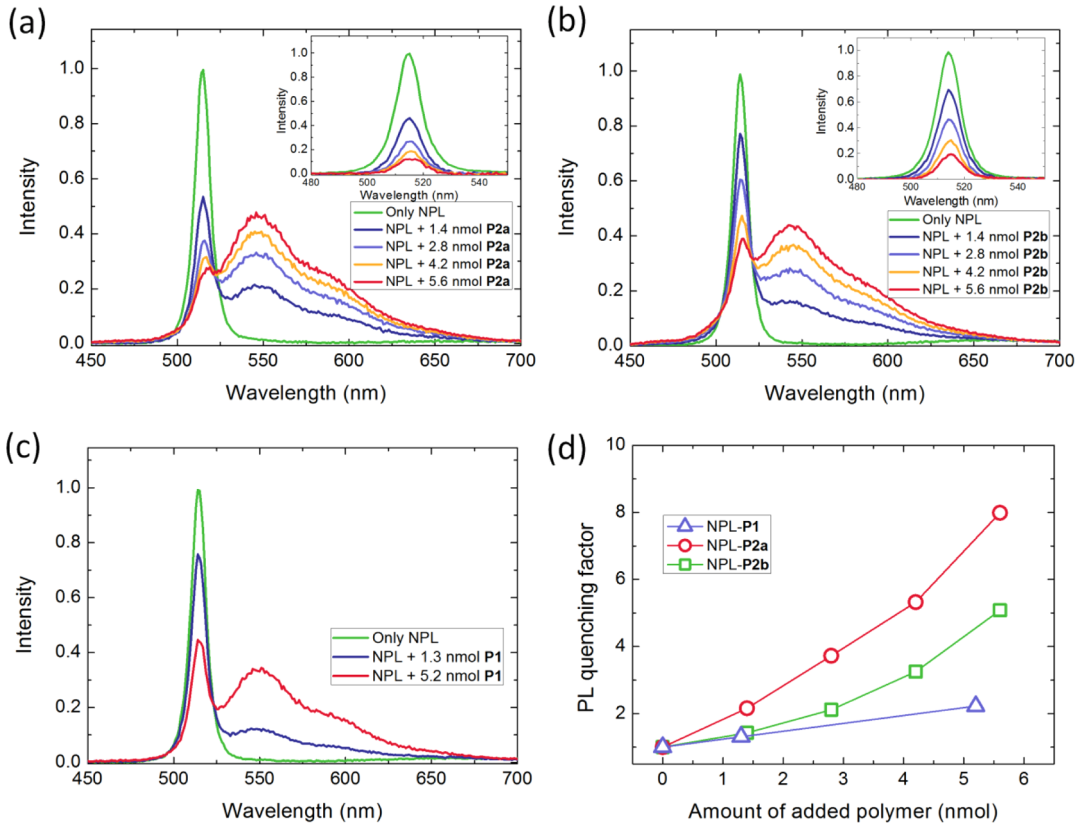


**Figure 4.** Steady-state photoluminescence spectra of the hybrids as the polymers were added step by step in the case of (a) NPL-**P2a**, (b) NPL-**P2b**, and (c) NPL-**P1** samples. The excitation wavelength for all cases was 375 nm. The insets in (a) and (b) show the NPL emission after spectral shape of the polymer emission has been subtracted. (d) Evolution of the NPL emission as a function of the added polymer amount for three different cases.

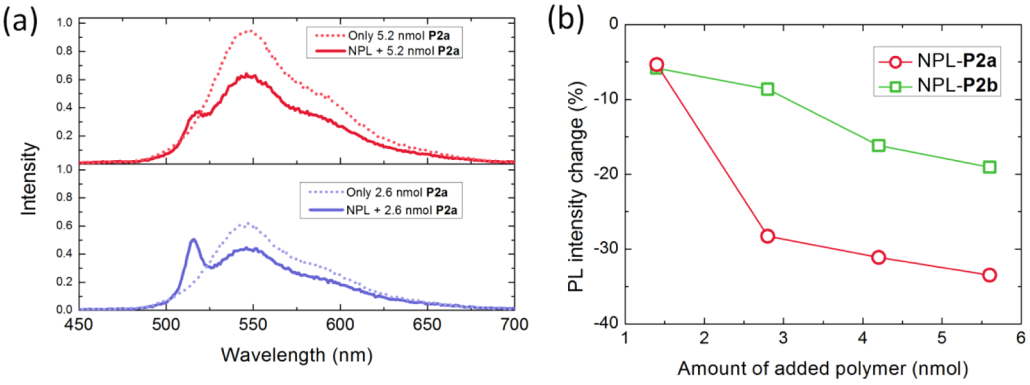


**Figure 5.** (a) Emission of the only polymer **P2a** and NPL + **P2a** for 5.2 nmol (top) and 2.6 nmol (bottom) polymer amounts. The excitation wavelength for all cases is 375 nm. (b) Emission intensity change in the polymers **P2a** and **P2b** in the presence of the NPLs as compared to bare polymer emission.

observed to further decrease (see Figure 4a,b). The insets in Figure 4a,b also show the evolution of the NPL emission after spectral profile of the polymer emission has been mathematically subtracted for each case. The precursor polymer (**P1**), which does not carry any specific anchor group but the same conjugated block, was also investigated as the negative control group (see Figure 4c). Addition of **P1** was observed to cause a decrease in the NPL emission, which was, however, weaker than that observed with **P2a** and **P2b**. Figure 4d summarizes the change in the NPL emission as a function of the increasing polymer amounts. In the case of reference polymer **P1**, the quenching of the NPL was found to be up to 2-fold. This decrease in the NPL emission can be well explained by the optical absorption of the NPL emission by the polymer since there is a nonzero absorbance of polymers at the emission peak of the NPLs (see Figure 3b for the absorbance of the polymers). We measured the absorbance of the polymer **P1** as ~0.30 at 512 nm, when 5.2 nmol of **P1** was added to the solution. The absorbance of **P2a** and **P2b** was also measured ~0.32 when 5.6 nmol of these polymers was added to the solution. According to the relation $\phi_{\text{transmitted}} = \phi_{\text{incident}} \times 10^{-A}$, where $\phi$ is the light intensity and $A$ is the measured absorbance (in log scale). For $A = 0.30$, one could simply calculate a 2-fold decrease (i.e., 50% change) in the NPL emission due to the absorption by the polymer. Therefore, this explains the decreased NPL emission with the addition of polymer **P1**.



DOI: 10.1021/acs.jpcc.5b12661
J. Phys. Chem. C 2016, 120, 3573−3582

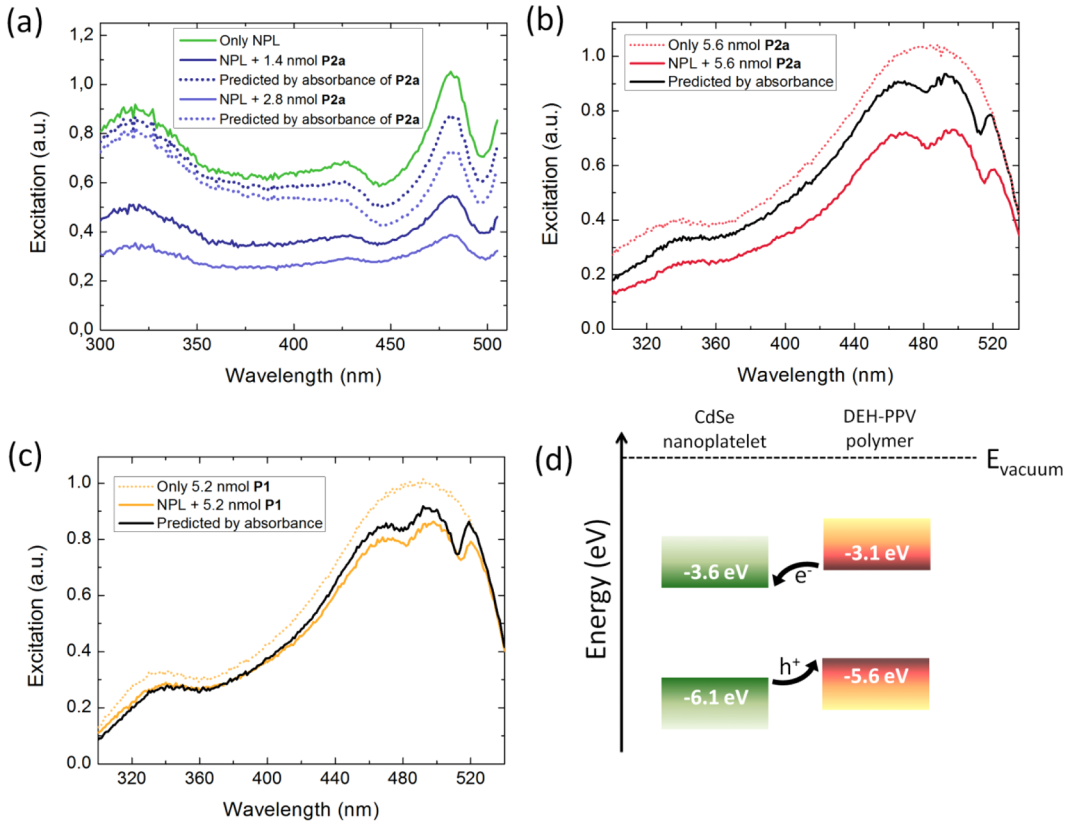


**Figure 6.** (a) Excitation spectra of the NPL emission for three different samples: only NPL (green), NPL + 1.4 nmol **P2a** (dark blue), and NPL + 2.8 nmol **P2a** (light blue). Excitation of the NPL emission is estimated by considering absorption of the excitation light by the **P2a** for two different cases (dotted curves). (b) Excitation spectra of the **P2a** for only 5.6 nmol **P2a** (red dotted curve) and NPL + 5.6 nmol **P2a** (red solid curve) samples. Also, excitation of the **P2a** emission is estimated by considering absorption of the excitation light by the NPLs (black solid curve). (c) Excitation spectra of the **P1** for only 5.2 nmol **P1** (orange dotted curve) and NPL + 5.2 nmol **P1** (orange solid curve) samples. Also, excitation of the **P1** emission is estimated by considering absorption of the excitation light by the NPLs (black solid curve). (d) Energy bands of the NPLs and polymers exhibiting a staggered (type II) band alignment favoring exciton dissociation.

In the case of polymers with anchor groups, the PL quenching was found to be much stronger than that caused by **P1**. With polymer **P2b** (having amine anchor), we observe that the quenching of the NPL emission was up to 5-fold (80% decrease in the NPL emission). Moreover, polymer **P2a** carrying the sulfide anchor shows the largest quenching in the NPL emission, a factor larger than 8 (~90% decrease in the NPL emission). Therefore, strong quenching of the NPL emission in the presence of functional polymers (**P2a** and **P2b**) strongly suggests that an additional process exists in addition to merely optical absorption of the polymers.

There exists a spectral overlap between the NPL emission and the polymer absorption. Thus, Förster resonance energy transfer (FRET) may be possible in these hybrids, and FRET might be the underlying process that can explain the emission quenching in the NPLs. To check this hypothesis with FRET, we investigated and analyzed steady-state PL emission of the polymers. In FRET process, the emission of the donor is decreased while the emission of the acceptor is concomitantly increased due to exciton transfer from the donor to the acceptor.[46−48] Therefore, we looked for a sign of an increased polymer emission as a result of possible FRET. Figure 5a shows the emission spectra of polymer **P2a** emission in the absence (dotted line) and presence (solid line) of the NPLs when excited at 375 nm. The only **P2a** emission was larger than the polymer emission in NPL-**P2a** samples for two different polymer amounts. This simply rules out the possibility of FRET as the dominant process behind the PL quenching in the NPLs. Also, Figure 5b illustrates the overall change of the emission intensity in the functional polymers **P2a** and **P2b** as a function of the added polymer amount (calculated from the emission spectra measured under excitation of 375 nm). Both polymers exhibit a decreased emission when mixed with the NPLs. The decrease in the polymer emission was larger for **P2a** than that of **P2b** (see Figure 5b). We also observed a larger quenching in the NPL emission in the case of **P2a** polymer.

To explain the emission quenching of both the NPLs and the polymers when mixed together, we consider another hypothesis, which is the exciton dissociation at the NPL−polymer interface. Exciton dissociation is expected to decrease radiative emission since free carriers are generated instead of exciton recombination. Previously, DEH-PPV-based polymers have been shown to be effective electron donors through exciton dissociation at the organic−organic interfaces with C60 molecules.[49] To check out the possibility of exciton dissociation in polymer/NPL hybrids, we looked into the excitation spectra of the NPLs and the polymers. Figure 6a shows the excitation spectra of the NPL peak emission at 513 nm for three different cases: only NPL, NPL + 1.4 nmol **P2a**, and NPL + 2.8 nmol **P2a** samples. To analyze the decrease in the excitation spectra of the NPL emission, first we consider the absorption of the excitation light by the **P2a**. Using the measured absorbance spectrum of the **P2a**, we calculated the decreased excitation light intensity by the following relation: $\phi_{\text{transmitted}} = \phi_{\text{incident}} \times$



DOI: 10.1021/acs.jpcc.5b12661
J. Phys. Chem. C 2016, 120, 3573−3582

$10^{-A}$. Then, we estimated the decrease in the NPL's excitation spectra due to the polymer absorption as plotted by the dotted curves in Figure 6a for the NPL + 1.4 nmol **P2a** and NPL + 2.8 nmol **P2a** samples. We observe that the experimentally measured excitation spectrum of the NPL emission in the presence of **P2a** is lower than the estimated excitation spectra. The excitation spectra of the NPLs showed a broadband quenching as the polymer amount was increased in the hybrid. This indicates that excitons formed in the NPLs are quenched independent of the excitation wavelength. This may suggest the possibility of a photoinduced charge transfer from the NPL into the polymer through exciton dissociation at the interface. In Figure 6b, we also present the excitation spectra of the polymer **P2a** emission measured at its peak emission wavelength of 545 nm in two different cases: only 5.6 nmol **P2a** and NPL + 5.6 nmol **P2a**. Here we also observed a broadband decrease in the excitation spectrum of the polymer when the polymer was mixed with the NPLs.

To analyze the decrease in the excitation spectra of the **P2a** emission, we also consider the absorption of the excitation light by the NPLs using the same methodology in Figure 6a. We estimated the decrease in the polymer's excitation spectra due to the NPL absorption, which is plotted by the black solid curve in Figure 6b. We observe that experimentally measured excitation spectra of the **P2a** emission in the presence of the NPLs (red solid curve) are still much lower than the estimated excitation spectra (black solid curve). Moreover, for excitation wavelengths longer than 520 nm, where there is no NPL absorbance, the excitation spectrum of the **P2a** also shows decreased intensity in the hybrid sample as compared to the estimated excitation. These observations strongly suggest that the excitons in the polymer **P2a** are also dissociated at the polymer/NPL interface, possibly via photoinduced electron transfer from the polymer.

As a control sample, we also tested the excitation spectra of the polymer **P1** before and after being mixed with the NPLs. Figure 6c shows the excitation spectra of only 5.2 nmol **P1** and NPL + 5.2 nmol **P1** samples. Here, we observed that the black curve (calculated excitation spectrum by considering absorption of the excitation light by the NPLs) and the orange curve (experimental excitation spectrum of the polymer in the presence of the NPLs) show a very good agreement as depicted in Figure 6c. Therefore, this strongly supports our view that the change in the excitation of the **P1** polymer just arises from the NPL absorption since there is no considerable near-field interactions between the species (**P1** and the NPLs) in the solution phase. However, in the case of **P2a**, there have to be near-field interactions (i.e., exciton dissociation) between the species to explain the observed changes. Also, Figure S8 shows the spectral quenching of excitation spectrum of the NPL and **P2a**, which shows a flat spectral response arising from the reciprocal exciton dissociation (hole transfer from the NPL and electron transfer from the polymer) at the organic−inorganic interface, which is independent of the excitation wavelength as long as it is above the bandgap of the material.

To further support exciton dissociation at the NPL−polymer interfaces, we investigated the energy band alignment between the NPLs and polymers. For this, we applied cyclic voltammetry (CV) to determine the energy levels of the polymers. From the CV data, the onset potentials for oxidation and reduction are found to be $E^{Ox}$ = 0.5 V and $E^{Red}$ = −2.0 V vs $Fc/Fc^+$. Thus, with an assumed level of the $Fc/Fc^+$ redox couple of −5.1 eV versus the vacuum, the HOMO and LUMO energy levels are calculated to be −5.6 and −3.1 eV, respectively (see Figure S1).[50] Previously, the conduction and valence band levels have been measured via ultraviolet photoelectron spectroscopy (UPS) in 4 ML thick CdSe NPLs as −3.6 and −6.1 eV, respectively.[51] The resulting band alignment at the polymer−NPL hybrids is illustrated in Figure 6d, which exhibits a staggered (i.e., type-II-like) band alignment. Therefore, exciton dissociation is expected to be favored via hole transfer to the polymer and electron transfer to the NPLs (see Figure 6d). On the basis of these observations, we can propose that exciton dissociation in the NPL−polymer hybrids is the dominant process.

Considering Figure 4a, which summarizes the emission quenching in the NPLs as a function of the added polymer amount for different polymers, **P2a** (functional polymer with the sulfide anchor) is observed to cause stronger quenching in the NPL emission than **P2b** (functional polymer with the amine anchor) while the ligand lengths are the same. This may suggest that **P2a** has a higher tendency to bind to the NPL surfaces than **P2b**. Thus, the emission of more NPLs could be quenched in the solution phase with more attached **P2a** due to exciton dissociation. Another possibility for the stronger quenching might be that sulfide anchors could create surface traps in the NPLs leading to nonradiative decay of the excitons. Such emission quenching arising from ligands in the nanocrystals have been shown previously.[15,24] Generally, thiol-based ligands were shown to create midgap trap states in the quantum dots causing charge trapping and emission quenching.[15] However, we also observed a larger emission quenching of the polymer **P2a** emission as compared to **P2b** as shown in Figure 5b. Thus, this opposes the possibility that the sulfide anchor might act as quencher, but most likely it acts as a stronger agent for hybridization with the NPLs than amine-based anchors. Moreover, enhanced interaction of **P2a** with the CdSe NPLs would explain the stronger PL quenching on both sides of the hybrid via exciton dissociating type-II interfaces.

Previously, exciton dissociation via ultrafast electron transfer (<1 ps) from the conjugated polymer into the colloidal quantum dots have been shown feasible.[52,53] Thus, this could make it possible for nanocrystals to replace commonly used electron acceptors such as C60. However, hole transfer from the spherical quantum dots into conjugated polymers has been generally found to be limited arising from its slow rate.[53] On the basis of our observations, which suggest efficient exciton dissociation in the NPLs through hole transfer into the conjugated polymers, we believe that atomically flat nanoplatelets might stand out as a more promising candidate for conjugated polymer−nanocrystal hybrids. The favorable geometry of the nanoplatelets arising from their large and flat surfaces may enable more efficient and faster hole transfer rates into organic semiconductors as predicted here.

In addition to different anchor types, we also investigated the effect of the ligand size on the optical properties of the resulting hybrids. For this, we developed **P2b** and **P2c** polymers both having amine-based anchors but with different sizes. **P2c** has an amino anchor that has a larger size than that of **P2b** polymer as shown in Figure 1. Figure 7 shows the emission spectra of the NPL + 9 nmol **P2b** and NPL + 9 nmol **P2c** samples. As presented in the inset of Figure 7, after the spectral profile of the polymer emission is subtracted mathematically, we observe that quenching of the NPL emission is found larger in **P2b**. The quenching factor of the NPL emission was calculated to be 11.3 and 6.8 for **P2b** and **P2c**, respectively. This also suggests that


DOI: 10.1021/acs.jpcc.5b12661
J. Phys. Chem. C 2016, 120, 3573−3582

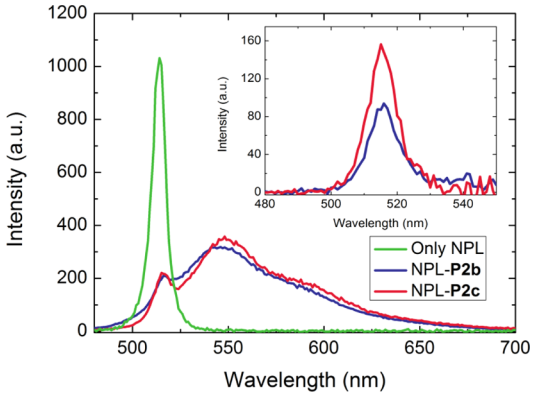


**Figure 7.** Emission spectra of the only NPL, NPL + 9 nmol **P2b**, and NPL + 9 nmol **P2c** samples. The inset shows the NPL emission after spectral profile of the polymer emission is subtracted. The emission quenching is larger for **P2b** than **P2c** since **P2b** has a shorter anchor ligand.

shorter ligands are more efficient for exciton dissociation. The charge transfer process, which generally occurs for distances shorter than 1 nm, is highly distance sensitive. Therefore, slight increase in the ligand size (as in the case of **P2c** polymer) can decrease the exciton dissociation efficiencies considerably.

Finally, we studied the solid-film morphology of the hybrids and found that hybrids exhibit homogeneously distributed NPLs in their solid films. For this, we prepared solutions with only NPL and NPL/**P2a** samples. Figure 8a shows HAADF-STEM images of the NPLs before they are mixed with the functional polymers. The NPLs on their own tend to exhibit aggregation while drying their solvent, which also leads to stacking of the NPLs via strong van der Waals forces. In the case of NPL/**P2a** hybrid sample, Figure 8b shows highly uniform distribution of the NPLs without any considerable aggregation although the same amount of NPLs have been employed. This suggests that the functional polymers bind to the NPL surfaces and help creating an increased separation between the NPLs so that NPL-to-NPL interactions could significantly be reduced. Such hybrids could be utilized for hybrid optoelectronic applications. The homogeneous distribution of the NPLs would be useful for efficient exciton dissociation in solar cells or exciton injection in light-emitting diodes.

## 4. CONCLUSION

Here, we introduced a hybrid conjugated polymer/nanoplatelet system for the first time, which exhibits strong photoluminescence quenching in their dilute solutions. The quenching has been explained with exciton dissociation at Type-II-like band alignment at the organic−inorganic interfaces. As compared to commonly studied polymer/quantum dot systems, where hole transfer has been limited from the quantum dots, uniquely enabled by atomically flat and large surface area nanoplatelets, the proposed composite system offers the opportunity to substantially enhance hole transfer into the polymers, as suggested by the steady state spectroscopy here. Thus, this work is expected to initiate future investigations based on ultrafast transient optical probes to capture the details of charge transfer kinetics in the hybrid organic−inorganic systems of colloidal nanoplatelets. As an important architectural feature of the proposed organic−inorganic composite, we found out that anchor type is effective for the hybridization efficiency. To this end, sulfide-based anchors showed a stronger binding affinity to the NPL surfaces as compared to amine-based anchors. Also, shorter ligands with the same anchor led to more efficient exciton dissociation thanks to closer integration of the polymers to the NPL surfaces. These findings indicate that the proposed organic−inorganic hybrids, which also allow for uniform NPL distribution in their solid thin-films, are very promising for hybrid optoelectronics, particularly in solar cells.

## ■ ASSOCIATED CONTENT

### Supporting Information

The Supporting Information is available free of charge on the ACS Publications website at DOI: 10.1021/acs.jpcc.5b12661.

Additional information on the detailed polymer characterization (cyclic voltammetry, FTIR spectrum, $^1$H NMR spectra of the functionalized polymers and their

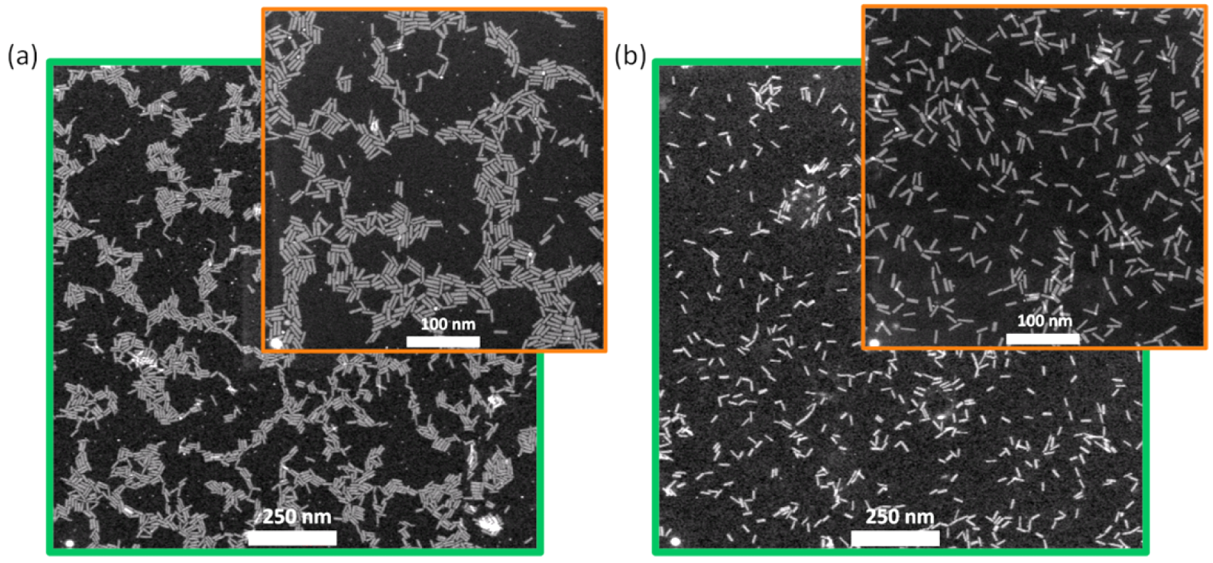


**Figure 8.** HAADF-STEM images of (a) only NPLs and (b) NPL-**P2a** hybrids. The insets show zoomed-in images with scale bar of 100 nm.



DOI: 10.1021/acs.jpcc.5b12661
J. Phys. Chem. C 2016, 120, 3573−3582

molecular weights) and quenching of the excitation spectra of the NPLs and polymer (PDF)

## AUTHOR INFORMATION


### Corresponding Author

*E-mail: hvdemir@ntu.edu.sg, volkan@bilkent.edu.tr (H.V.D.)

### Author Contributions

B.G. and F.M. contributed equally to this work.


### Notes

The authors declare no competing financial interest.

## ACKNOWLEDGMENTS

The authors gratefully thank the Deutsche Forschungsgemeinschaft (DFG): International Research Training Group (IRTG) 1404 "Self-Organized Materials for Optoelectronics" for funding. The authors also thank the following funding agencies for financial support: EU-FP7 Nanophotonics4Energy NoE, and TUBITAK EEEAG 109E002, 109E004, 110E010, 110E217, ESF-EURYI, TUBA-GEBIP, and in part from NRF-RF-2009-09, NRF-CRP-6-2010-02, A*STAR of Singapore and EPSRC (EP/I029141). H.V.D. acknowledges support from ESF-EURYI and TUBA.

## ABBREVIATIONS

DCM, dichloromethane; DEH-PPV, poly[2,5-di(2′-ethylhexyloxy)-1,4-phenylenevinylene]; FTIR, Fourier transform infrared; NMR, nuclear magnetic resonance; OEH, 2-ethylhexyloxy; $M_n$, number-average molar mass; PDI, polydispersity index; PPV, poly(*p*-phenylenevinylene); ROMP, ring-opening metathesis polymerization.

## REFERENCES


(1) Huynh, W. U.; Dittmer, J. J.; Alivisatos, A. P. Hybrid Nanorod-Polymer Solar Cells. *Science* **2002**, *295* (5564), 2425−2427.

(2) He, M.; Qiu, F.; Lin, Z. Toward High-Performance Organic−Inorganic Hybrid Solar Cells: Bringing Conjugated Polymers and Inorganic Nanocrystals in Close Contact. *J. Phys. Chem. Lett.* **2013**, *4* (11), 1788−1796.

(3) Reiss, P.; Couderc, E.; De Girolamo, J.; Pron, A. Conjugated Polymers/semiconductor Nanocrystals Hybrid Materials–Preparation, Electrical Transport Properties and Applications. *Nanoscale* **2011**, *3* (2), 446−489.

(4) Wright, M.; Uddin, A. Organic—inorganic Hybrid Solar Cells: A Comparative Review. *Sol. Energy Mater. Sol. Cells* **2012**, *107*, 87−111.

(5) Guzelturk, B.; Demir, H. V. Organic-Inorganic Composites of Semiconductor Nanocrystals For Efficient Excitonics. *J. Phys. Chem. Lett.* **2015**, *6*, 2206−2215.

(6) Guzelturk, B.; Hernandez Martinez, P. L.; Sharma, V. K.; Coskun, Y.; Ibrahimova, V.; Tuncel, D.; Govorov, A. O.; Sun, X. W.; Xiong, Q.; Demir, H. V.; et al. Study of Exciton Transfer in Dense Quantum Dot Nanocomposites. *Nanoscale* **2014**, *6* (19), 11387−11394.

(7) Kwak, J.; Bae, W. K.; Zorn, M.; Woo, H.; Yoon, H.; Lim, J.; Kang, S. W.; Weber, S.; Butt, H.-J. H.-J.; Zentel, R.; et al. Characterization of Quantum Dot/conducting Polymer Hybrid Films and Their Application to Light-Emitting Diodes. *Adv. Mater.* **2009**, *21* (48), 5022−5026.

(8) Zorn, M.; Bae, W. K.; Kwak, J.; Lee, H.; Lee, C.; Zentel, R.; Char, K. Quantum Dot-Block Copolymer Hybrids with Improved Properties and Their Application to Quantum Dot Light-Emitting Devices. *ACS Nano* **2009**, *3* (5), 1063−1068.

(9) Chin, P. T. K.; Hikmet, R. A. M.; Janssen, R. A. J. Energy Transfer in Hybrid Quantum Dot Light-Emitting Diodes. *J. Appl. Phys.* **2008**, *104* (1), 013108.

(10) Holder, E.; Tessler, N.; Rogach, A. L. Hybrid Nanocomposite Materials with Organic and Inorganic Components for Opto-Electronic Devices. *J. Mater. Chem.* **2008**, *18* (10), 1064.

(11) Mutlugun, E.; Guzelturk, B.; Abiyasa, A. P.; Gao, Y.; Sun, X. W.; Demir, H. V. Colloidal Quantum Dot Light-Emitting Diodes Employing Phosphorescent Small Organic Molecules as Efficient Exciton Harvesters. *J. Phys. Chem. Lett.* **2014**, *5* (16), 2802−2807.

(12) Zhou, R.; Stalder, R.; Xie, D.; Cao, W.; Zheng, Y.; Yang, Y.; Plaisant, M.; Holloway, P. H.; Schanze, K. S.; Reynolds, J. R.; et al. Enhancing the Efficiency of Solution-Processed Polymer:Colloidal Nanocrystal Hybrid Photovoltaic Cells Using Ethanedithiol Treatment. *ACS Nano* **2013**, *7* (6), 4846−4854.

(13) Liu, Z.; Sun, Y.; Yuan, J.; Wei, H.; Huang, X.; Han, L.; Wang, W.; Wang, H.; Ma, W. High-Efficiency Hybrid Solar Cells Based on polymer/PbSx Se1-X Nanocrystals Benefiting from Vertical Phase Segregation. *Adv. Mater.* **2013**, *25* (40), 5772−5778.

(14) Scharber, M. C.; Mühlbacher, D.; Koppe, M.; Denk, P.; Waldauf, C.; Heeger, A. J.; Brabec, C. J. Design Rules for Donors in Bulk-Heterojunction Solar Cells—Towards 10% Energy-Conversion Efficiency. *Adv. Mater.* **2006**, *18* (6), 789−794.

(15) Greaney, M. J.; Brutchey, R. L. Ligand Engineering in Hybrid Polymer:nanocrystal Solar Cells. *Mater. Today* **2015**, *18* (1), 31−38.

(16) Greenham, N.; Peng, X.; Alivisatos, A. Charge Separation and Transport in Conjugated-Polymer/semiconductor-Nanocrystal Composites Studied by Photoluminescence Quenching and Photoconductivity. *Phys. Rev. B: Condens. Matter Mater. Phys.* **1996**, *54* (24), 17628−17637.

(17) Martínez-Ferrero, E.; Albero, J.; Palomares, E. Materials, Nanomorphology, and Interfacial Charge Transfer Reactions in Quantum Dot/Polymer Solar Cell Devices. *J. Phys. Chem. Lett.* **2010**, *1* (20), 3039−3045.

(18) Tang, J.; Kemp, K. W.; Hoogland, S.; Jeong, K. S.; Liu, H.; Levina, L.; Furukawa, M.; Wang, X.; Debnath, R.; Cha, D.; et al. Colloidal-Quantum-Dot Photovoltaics Using Atomic-Ligand Passivation. *Nat. Mater.* **2011**, *10* (10), 765−771.

(19) Tomczak, N.; Jańczewski, D.; Han, M.; Vancso, G. J. Designer Polymer−quantum Dot Architectures. *Prog. Polym. Sci.* **2009**, *34* (5), 393−430.

(20) Soreni-Harari, M.; Yaacobi-Gross, N.; Steiner, D.; Aharoni, A.; Banin, U.; Millo, O.; Tessler, N. Tuning Energetic Levels in Nanocrystal Quantum Dots through Surface Manipulations. *Nano Lett.* **2008**, *8* (2), 678−684.

(21) Munro, A. M.; Zacher, B.; Graham, A.; Armstrong, N. R. Photoemission Spectroscopy of Tethered CdSe Nanocrystals: Shifts in Ionization Potential and Local Vacuum Level as a Function of Nanocrystal Capping Ligand. *ACS Appl. Mater. Interfaces* **2010**, *2* (3), 863−869.

(22) Mathias, F.; Fokina, A.; Landfester, K.; Tremel, W.; Schmid, F.; Char, K.; Zentel, R. Morphology Control in Biphasic Hybrid Systems of Semiconducting Materials. *Macromol. Rapid Commun.* **2015**, *36* (11), 959−983.

(23) Munro, A. M.; Jen-LaPlante, I.; Ng, M. S.; Ginger, D. S. Quantitative Study of the Effects of Surface Ligand Concentration on CdSe Nanocrystal Photoluminescence. *J. Phys. Chem. C* **2007**, *111* (17), 6220−6227.

(24) Knowles, K. E.; Tice, D. B.; McArthur, E. A.; Solomon, G. C.; Weiss, E. A. Chemical Control of the Photoluminescence of CdSe Quantum Dot−Organic Complexes with a Series of Para-Substituted Aniline Ligands. *J. Am. Chem. Soc.* **2010**, *132* (3), 1041−1050.

(25) Günes, S.; Neugebauer, H.; Sariciftci, N. S. Conjugated Polymer-Based Organic Solar Cells. *Chem. Rev.* **2007**, *107* (4), 1324−1338.

(26) Ren, S.; Chang, L.-Y.; Lim, S.-K.; Zhao, J.; Smith, M.; Zhao, N.; Bulović, V.; Bawendi, M.; Gradecak, S. Inorganic-Organic Hybrid Solar Cell: Bridging Quantum Dots to Conjugated Polymer Nanowires. *Nano Lett.* **2011**, *11* (9), 3998−4002.

(27) Lhuillier, E.; Pedetti, S.; Ithurria, S.; Nadal, B.; Heuclin, H.; Dubertret, B. Two-Dimensional Colloidal Metal Chalcogenides




DOI: 10.1021/acs.jpcc.5b12661
*J. Phys. Chem. C* 2016, 120, 3573−3582

Semiconductors: Synthesis, Spectroscopy, and Applications. *Acc. Chem. Res.* **2015**, *48* (1), 22−30.
(28) Ithurria, S.; Tessier, M. D.; Mahler, B.; Lobo, R. P. S. M.; Dubertret, B.; Efros, A. L. Colloidal Nanoplatelets with Two-Dimensional Electronic Structure. *Nat. Mater.* **2011**, *10* (12), 936−941.
(29) Olutas, M.; Guzelturk, B.; Kelestemur, Y.; Yeltik, A.; Delikanli, S.; Demir, H. V. Lateral Size-Dependent Spontaneous and Stimulated Emission Properties in Colloidal CdSe Nanoplatelets. *ACS Nano* **2015**, *9* (5), 5041−5050.
(30) Chen, Z.; Nadal, B.; Mahler, B.; Aubin, H.; Dubertret, B. Quasi-2D Colloidal Semiconductor Nanoplatelets for Narrow Electroluminescence. *Adv. Funct. Mater.* **2014**, *24* (3), 295−302.
(31) Guzelturk, B.; Kelestemur, Y.; Olutas, M.; Delikanli, S.; Demir, H. V. Amplified Spontaneous Emission and Lasing in Colloidal Nanoplatelets. *ACS Nano* **2014**, *8* (7), 6599−6605.
(32) Grim, J. Q.; Christodoulou, S.; Di Stasio, F.; Krahne, R.; Cingolani, R.; Manna, L.; Moreels, I. Continuous-Wave Biexciton Lasing at Room Temperature Using Solution-Processed Quantum Wells. *Nat. Nanotechnol.* **2014**, *9* (11), 891−895.
(33) Lhuillier, E.; Dayen, J.-F.; Thomas, D. O.; Robin, A.; Doudin, B.; Dubertret, B. Nanoplatelets Bridging a Nanotrench: A New Architecture for Photodetectors with Increased Sensitivity. *Nano Lett.* **2015**, *15* (3), 1736−1742.
(34) Lhuillier, E.; Robin, A.; Ithurria, S.; Aubin, H.; Dubertret, B. Electrolyte-Gated Colloidal Nanoplatelets-Based Phototransistor and Its Use for Bicolor Detection. *Nano Lett.* **2014**, *14*, 2715−2719.
(35) Wu, K.; Li, Q.; Du, Y.; Chen, Z.; Lian, T. Ultrafast Exciton Quenching by Energy and Electron Transfer in Colloidal CdSe nanosheet−Pt Heterostructures. *Chem. Sci.* **2015**, *6* (2), 1049−1054.
(36) Guzelturk, B.; Olutas, M.; Delikanli, S.; Kelestemur, Y.; Erden, O.; Demir, H. V. Nonradiative Energy Transfer in Colloidal CdSe Nanoplatelet Films. *Nanoscale* **2015**, *7* (6), 2545−2551.
(37) Rowland, C. E.; Fedin, I.; Zhang, H.; Gray, S. K.; Govorov, A. O.; Talapin, D. V.; Schaller, R. D. Picosecond Energy Transfer and Multiexciton Transfer Outpaces Auger Recombination in Binary CdSe Nanoplatelet Solids. *Nat. Mater.* **2015**, *14*, 484−489.
(38) Guzelturk, B.; Erdem, O.; Olutas, M.; Kelestemur, Y.; Demir, H. V. Stacking in Colloidal Nanoplatelets: Tuning Excitonic Properties. *ACS Nano* **2014**, *8* (12), 12524−12533.
(39) zur Borg, L.; Domanski, A. L.; Berger, R.; Zentel, R. Photoinduced Charge Separation of Self-Organized Semiconducting Superstructures Composed of a Functional Polymer-TiO 2 Hybrid. *Macromol. Chem. Phys.* **2013**, *214* (9), 975−984.
(40) Sirringhaus, H.; Brown, P. J.; Friend, R. H.; Nielsen, M. M.; Bechgaard, K.; Langeveld-Voss, B. M. W.; Spiering, A. J. H.; Janssen, R. A. J.; Meijer, E. W.; Herwig, P.; et al. Two-Dimensional Charge Transport in Self-Organized, High-Mobility Conjugated Polymers. *Nature* **1999**, *401* (6754), 685−688.
(41) Rajh, T.; Chen, L. X.; Lukas, K.; Liu, T.; Thurnauer, M. C.; Tiede, D. M. Surface Restructuring of Nanoparticles: An Efficient Route for Ligand−Metal Oxide Crosstalk. *J. Phys. Chem. B* **2002**, *106* (41), 10543−10552.
(42) Mathias, F.; Tahir, M. N.; Tremel, W.; Zentel, R. Functionalization of TiO 2 Nanoparticles with Semiconducting Polymers Containing a Photocleavable Anchor Group and Separation via Irradiation Afterward. *Macromol. Chem. Phys.* **2014**, *215* (7), 604−613.
(43) Menk, F.; Mondeshki, M.; Dudenko, D.; Shin, S.; Schollmeyer, D.; Ceyhun, O.; Choi, T.-L.; Zentel, R. Reactivity Studies of Alkoxy-Substituted [2.2]Paracyclophane-1,9-Dienes and Specific Coordination of the Monomer Repeating Unit during ROMP. *Macromolecules* **2015**, *48* (20), 7435−7445.
(44) She, C.; Fedin, I.; Dolzhnikov, D. S.; Demortière, A.; Schaller, R. D.; Pelton, M.; Talapin, D. V.; Richard, D. Low-Threshold Stimulated Emission Using Colloidal Quantum Wells. *Nano Lett.* **2014**, *14* (5), 2772−2777.
(45) Abécassis, B.; Tessier, M. D.; Davidson, P.; Dubertret, B. Self-Assembly of CdSe Nanoplatelets into Giant Micrometer-Scale Needles Emitting Polarized Light. *Nano Lett.* **2014**, *14* (2), 710−715.
(46) Guzelturk, B.; Martinez, P. L. H.; Zhang, Q.; Xiong, Q.; Sun, H.; Sun, X. W.; Govorov, A. O.; Demir, H. V. Excitonics of Semiconductor Quantum Dots and Wires for Lighting and Displays. *Laser Photon. Rev.* **2014**, *8* (1), 73−93.
(47) Guzelturk, B.; Hernandez Martinez, P. L.; Zhao, D.; Sun, X. W.; Demir, H. V. Singlet and Triplet Exciton Harvesting in the Thin Films of Colloidal Quantum Dots Interfacing Phosphorescent Small Organic Molecules. *J. Phys. Chem. C* **2014**, *118* (45), 25964−25969.
(48) Lakowicz, J. R. *Principles of Fluorescence Spectroscopy*; Springer: Berlin, 2006.
(49) van der Veen, M. H.; de Boer, B.; Stalmach, U.; van de Wetering, K. I.; Hadziioannou, G. Donor−Acceptor Diblock Copolymers Based on PPV and C 60: Synthesis, Thermal Properties, and Morphology. *Macromolecules* **2004**, *37* (10), 3673−3684.
(50) Thompson, B. C.; Kim, Y.-G.; McCarley, T. D.; Reynolds, J. R. Soluble Narrow Band Gap and Blue Propylenedioxythiophene-Cyanovinylene Polymers as Multifunctional Materials for Photovoltaic and Electrochromic Applications. *J. Am. Chem. Soc.* **2006**, *128* (39), 12714−12725.
(51) Fan, F.; Kanjanaboos, P.; Saravanapavanantham, M.; Beauregard, E.; Ingram, G.; Yassitepe, E.; Adachi, M. M.; Voznyy, O.; Johnston, A. K.; Walters, G.; et al. Colloidal CdSe(1-x)S(x) Nanoplatelets with Narrow and Continuously-Tunable Electroluminescence. *Nano Lett.* **2015**, *15* (7), 4611−4615.
(52) Colbert, A. E.; Janke, E. M.; Hsieh, S. T.; Subramaniyan, S.; Schlenker, C. W.; Jenekhe, S. A.; Ginger, D. S. Hole Transfer from Low Band Gap Quantum Dots to Conjugated Polymers in Organic/Inorganic Hybrid Photovoltaics. *J. Phys. Chem. Lett.* **2013**, *4* (2), 280−284.
(53) Morgenstern, F. S. F.; Rao, A.; Böhm, M. L.; Kist, R. J. P.; Vaynzof, Y.; Greenham, N. C. Ultrafast Charge- and Energy-Transfer Dynamics in Conjugated Polymer: Cadmium Selenide Nanocrystal Blends. *ACS Nano* **2014**, *8* (2), 1647−1654.


DOI: 10.1021/acs.jpcc.5b12661
*J. Phys. Chem. C* 2016, 120, 3573−3582